# Magnetization Process of Atacamite: A Case of Weakly Coupled $S = 1/2$ Sawtooth Chains

L. Heinze,[1,*] H. O. Jeschke[ORCID],[2] I. I. Mazin[ORCID],[3,4] A. Metavitsiadis[ORCID],[5] M. Reehuis,[6] R. Feyerherm[ORCID],[6] J.-U. Hoffmann,[6]
M. Bartkowiak,[6] O. Prokhnenko[ORCID],[6] A. U. B. Wolter,[7] X. Ding[ORCID],[8] V. S. Zapf[ORCID],[8] C. Corvalán Moya[ORCID],[9,8] F. Weickert[ORCID],[8,†]
M. Jaime,[8,†] K. C. Rule,[10] D. Menzel[ORCID],[1] R. Valentí,[11] W. Brenig,[5] and S. Süllow[1]

[1]Institut für Physik der Kondensierten Materie, Technische Universität Braunschweig, D-38106 Braunschweig, Germany
[2]Research Institute for Interdisciplinary Science, Okayama University, Okayama 700-8530, Japan
[3]Department of Physics and Astronomy, George Mason University, Fairfax, Virginia 22030, USA
[4]Quantum Science and Engineering Center, George Mason University, Fairfax, Virginia 22030, USA
[5]Institut für Theoretische Physik, Technische Universität Braunschweig, D-38106 Braunschweig, Germany
[6]Helmholtz-Zentrum Berlin für Materialien und Energie GmbH, D-14109 Berlin, Germany
[7]Institute for Solid State and Materials Research, Leibniz IFW Dresden, D-01069 Dresden, Germany
[8]National High Magnetic Field Laboratory, Los Alamos National Laboratory, Los Alamos, New Mexico 87545, USA
[9]National Atomic Energy Commission (CNEA), Tres de Febrero University (UNTREF),
National Scientific and Technical Research Council (CONICET), Argentina
[10]Australian Nuclear Science and Technology Organisation, Lucas Heights, New South Wales 2234, Australia
[11]Institut für Theoretische Physik, Goethe-Universität Frankfurt, D-60438 Frankfurt am Main, Germany

We present a combined experimental and theoretical study of the mineral atacamite $Cu_2Cl(OH)_3$. Density-functional theory yields a Hamiltonian describing anisotropic sawtooth chains with weak 3D connections. Experimentally, we fully characterize the antiferromagnetically ordered state. Magnetic order shows a complex evolution with the magnetic field, while, starting at 31.5 T, we observe a plateaulike magnetization at about $M_{sat}/2$. Based on complementary theoretical approaches, we show that the latter is unrelated to the known magnetization plateau of a sawtooth chain. Instead, we provide evidence that the magnetization process in atacamite is a field-driven canting of a 3D network of weakly coupled sawtooth chains that form giant moments.

Frustrated low-dimensional quantum spin systems offer a unique opportunity to study complex quantum phases [1–4]. In the search for novel and exotic ground and field-induced states, such as spin liquids, magnetization plateaus, or nematic phases, a multitude of models have been studied, including the kagome lattice, the diamond chain, or the frustrated $J_1 - J_2$ chain [5–7]. Experimental efforts to identify materials to test these theoretical concepts are exemplified by work on natural minerals such as herbertsmithite, azurite, or linarite [8–13]. Through this combined effort, a new level of insight into complex topics of quantum magnetism is achieved.

The $\Delta$ chain, or sawtooth chain, represents one of the fundamental models of frustrated quantum magnetism. It consists of a chain of spin triangles, with the Hamiltonian

$$\mathcal{H} = \sum_i J\mathbf{S}_i \cdot \mathbf{S}_{i+2} + J'(\mathbf{S}_i \cdot \mathbf{S}_{i+1} + \mathbf{S}_{i+1} \cdot \mathbf{S}_{i+2}) - \mathbf{h} \cdot \mathbf{S}_i. \quad (1)$$

$\mathbf{S}_i$ represents a spin $S = 1/2$ at site $i$; the sites $i$ and $i + 2$ are neighbors in the chain "spine", while $J'$ is the interaction between spine sites and the sawteeth tips. $\mathbf{h}$ is the external magnetic field. This model has been studied theoretically for decades [14–34]. Real materials, however,

are inevitably more complex than this simplified model. Delafossite and euchroite have more than two relevant couplings [35,36], certain metalorganic systems have a ferromagnetic intraspine $J$ [27,37], and in $Rb_2NaTi_3F_{12}$ the $\Delta$ chain is coupled to an antiferromagnetic (AFM) chain [38]. In this Letter, based on a combined experimental and theoretical study of atacamite, $Cu_2Cl(OH)_3$, we show that its magnetic behavior originates from an intricate and rather unusual 3D connectivity of $\Delta$ chains, not previously addressed.

We have measured magnetization, magnetic susceptibility, and specific heat of atacamite in fields up to 13 T. Neutron scattering was carried out at the Helmholtz-Zentrum Berlin BER II reactor using the instruments E2, E5, and the High Field Magnet and Extreme Environment Diffractometer (HFM/EXED) for fields up to 25 T [39–41]. We have determined both the magnetic and crystallographic structures of our mineral single crystals [42,44–46]. In addition, we have performed a high-field magnetostriction and magnetization study in fields up to 65 T at the Pulsed Field Facility of the National High Magnetic Field Laboratory (NHMFL), Los Alamos. In the present Letter, we focus on data taken in magnetic fields applied along the crystallographic $b$ axis.
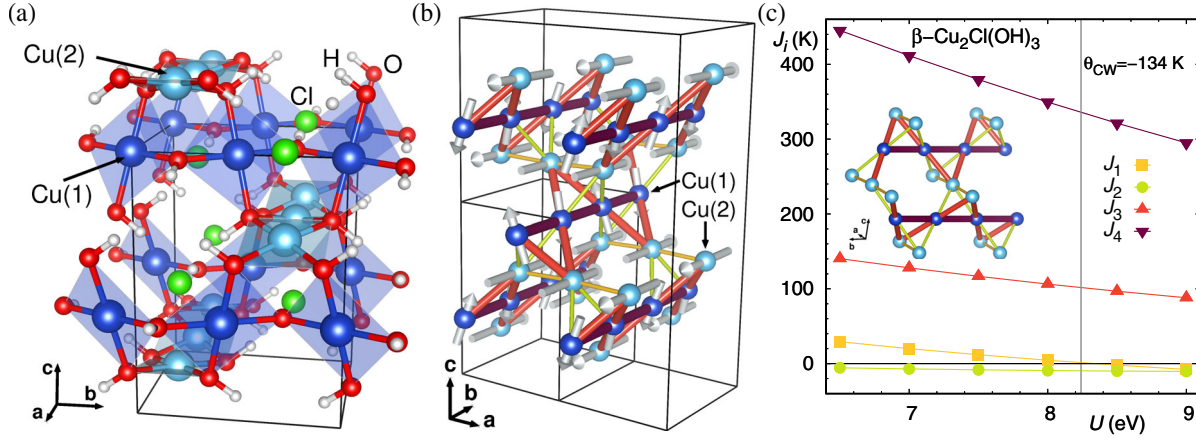
FIG. 1.   (a) Crystal structure of atacamite $Cu_2Cl(OH)_3$. (b) Visualization of the dominant magnetic exchange paths in atacamite forming a sawtooth pattern. Also shown is the magnetic structure together with the nuclear and the magnetic unit cell (black solid lines). (c) Cu-Cu exchange couplings of atacamite, $J_i$, with $i = 1, 2, \ldots$ denoting first, second, … neighbor. The vertical line indicates the $U$ value at which the couplings $J_1 = 1.3$, $J_2 = -9.6$, $J_3 = 102$, $J_4 = 336$, $J_{11b} = 15.6$, $J_{13} = 1.1$ K match the experimental Curie-Weiss temperature; for details, see text.

Atacamite magnetically orders at low temperatures and we found a complex field-induced spin reorientation behavior. Magnetic fields of ~30 T suppress the ordered state, taking the system to nearly half its saturation magnetization, where it persists up to the highest field reached in this study. To rationalize these results, we have investigated the electronic structure and magnetic interactions using density-functional theory (DFT) with full potential local orbital basis [47] and generalized gradient approximation (GGA) functional [48]; electronic correlations on $Cu^{2+}$ were accounted for by the GGA + $U$ method [49]. The Hamiltonian thus obtained consists of strongly coupled Cu $\Delta$ chains, forming a weakly coupled network. We consider the uncoupled chains in a magnetic field using infinite system time-evolving block decimation (iTEBD) [50] as well as exact diagonalization (ED). The results justify our subsequent evaluation of the magnetization process within a 3D mean-field approximation (MFA) and accounting for the interchain coupling.

Atacamite $Cu_2Cl(OH)_3$ crystallizes in a $Pnma$ orthorhombic structure [lattice constants $a = 6.02797$, $b = 6.86383$, $c = 9.11562$ Å; Fig. 1(a)] [42,51,52]. There are two inequivalent Cu sites which are drawn as dark [Cu(1)] and light [Cu(2)] blue spheres in Fig. 1(a)–1(c). Previously, this crystal structure was derived from a network of pyrochlore tetrahedra built up by $Cu^{2+}$ ions [52–54]. Our DFT calculations, however, indicate that the symmetry of the magnetic Hamiltonian is dramatically lower than the one anticipated from the bond lengths only. Indeed, the bonds derived from the first, second, and third pyrochlore coordination shells vary in length by ±10% within each set, but the calculated exchange parameters (corresponding to 4, 6, and 7 distinct Cu-Cu distances, respectively) vary by 2 orders of magnitude. As we show below, our calculated Hamiltonian provides an excellent explanation of the experimental observations.

First evidence of the existence of ordered magnetism in atacamite was reported previously [40,52–54]. Furthermore, we present zero-field specific heat measurements, with an anomaly indicating a magnetic transition at $T_N = 8.4$ K [Fig. 2(a)]. An antiferromagnetic anomaly is also observed at $T_N = 8.4$ K in the low-field (0.1 T) susceptibility as maximum in $d(\chi T)/dT$ [Fig. 2(b)] [55]. In neutron diffraction, we find magnetic intensity below a slightly higher $T_N = 8.9$ K with a magnetic propagation vector $\mathbf{q} = (1/2, 0, 1/2)$ [Fig. 2(c)].

We also detect an additional hump in the specific heat at $T \sim 5$ K [Fig. 2(a)], hinting at a more complex temperature
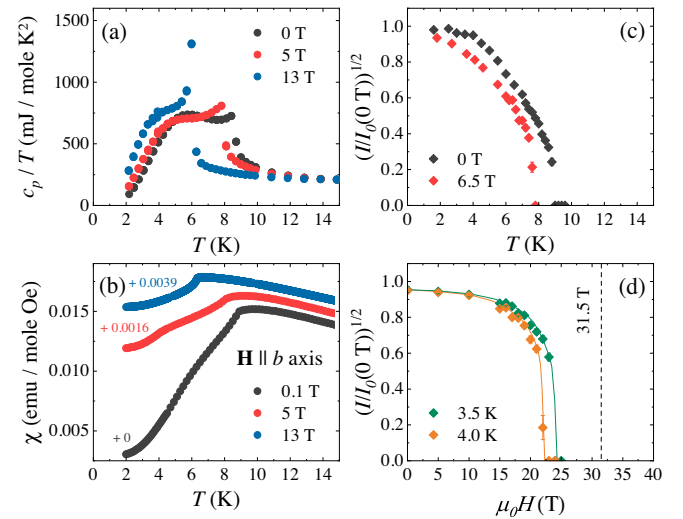


FIG. 2.   (a) Specific heat $c_p/T$, (b) magnetic susceptibility $\chi$, and normalized intensity of the $(1/2\,0\,1/2)_M$ neutron scattering reflection as function of (c) temperature and (d) magnetic field ($\mathbf{H}\|b$ axis). Data in (b) are shifted for clarity by values denoted in the plot; lines in (d) are guides to the eye; dashed line indicates the plateau field.

evolution of the magnetic state, involving, for instance, spin reorientations. A calculation of the magnetic entropy from our data (ignoring a phonon contribution) gives a value $\sim 0.65 R \ln(2)$ at $T_N$ [42]. Such a small value is typical for magnetically ordered states in frustrated magnets with the magnetic entropy being distributed over the temperature scale set by the dominant coupling strengths, here $J_4$ and $J_3$ [Fig. 1(c)].

In magnetic fields $\mathbf{H} \| b$, the features in the specific heat and the susceptibility are shifted to lower temperatures and the AFM anomaly is sharpened [Figs. 2(a) and 2(b)]. This shift is supported by neutron scattering in 6.5 T [Fig. 2(c)]. Field-dependent neutron scattering at the HFM/EXED instrument yields a suppression of AFM order at 24 T ($T = 3.5$ K) [Fig. 2(d)]. Altogether, an external magnetic field leads to a suppression of the AFM phase, with $T_N$ fully suppressed in $\sim$30 T.

The low-$T$ susceptibility in high fields is larger than in low fields [Fig. 2(b)]. It reflects a metamagnetic transition occurring at a few Tesla (see below). Since for the other crystallographic directions we find no such transition, it suggests that the $b$ axis is the easy magnetic axis and this is a spin-flop transition (see Supplemental Material [42]). This is consistent with our refined magnetic structure.

From the magnetic Bragg peak intensities, we derive the magnetic structure in Fig. 1(b) [42,56]. On the Cu(1) site, the ordered magnetic moments of 0.34(4) $\mu_B$ are arranged in a nearly perfect AFM pattern with the Cartesian components $\mu_{\mathrm{ord,Cu(1)}}(x, y, z) = [0.09(9), 0.04(2), 0.32(7)] \, \mu_B$. The ordering vector corresponds to alternating signs for the $x$ and $z$ moment components, while the $y$ component stays the same within the same chain. The angle between two Cu(1) neighbors is thus $\theta = 166.3°$, close to 180°. All Cu(2) sites carry a moment $\mu_{\mathrm{ord,Cu(2)}}(x, y, z) = [0, 0.59(2), 0] \, \mu_B$, where moments are parallel to $y$ within one set of sawtooth sites of a single chain (see details in Supplemental Material [42]).

To assess the magnetic phase diagram, we used magnetometry in pulsed magnetic fields for $\mathbf{H} \| b$ [57,58]. In Figs. 3(a) and 3(b), we summarize the magnetostriction and magnetization, respectively. Below $T_N$ and fields of $\mu_0 H_1 \lesssim 4$ T, a kink in the magnetization indicates a spin-flop transition. When increasing temperature, the kink becomes weaker and shifts to higher fields in the AFM phase [42]. For temperatures below $\sim$5 K, a weak shoulder appears [inset Fig. 3(b)], which corresponds to shallow minima in the magnetostriction [42]. This might indicate a splitting of the spin-flop transition due to a weak three-axes exchange anisotropy.

Immediately after the spin-flop transition, $M(H)$ grows linearly with $dM/dH \approx 0.013 \, \mu_B /$ T, but starts bending upward up to a field of $\mu_0 H_2 = 31.5$ T, where the slope reaches 0.042 $\mu_B /$ T [Fig. 3(b)]. After that, a wide magnetization plateaulike behavior at about 0.45 $\mu_B$/Cu sets in. The plateau, also detected in the magnetostriction [Fig. 3(a)],


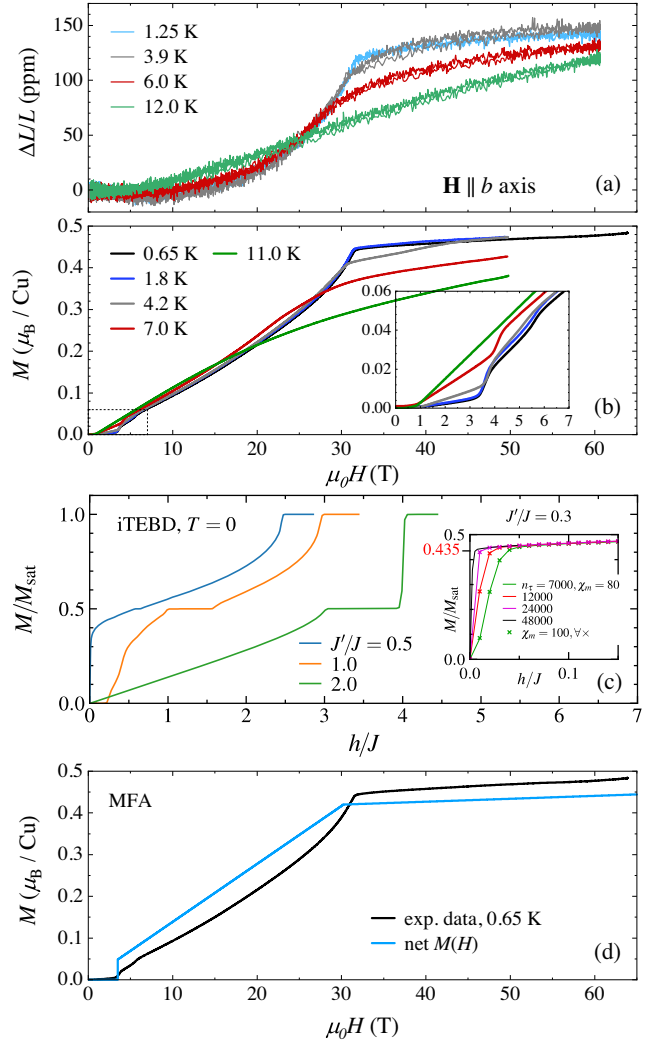
FIG. 3. (a) Magnetostriction and (b) magnetization of atacamite in magnetic fields $\mathbf{H} \| b$ axis at different temperatures. (c) Magnetization versus $h$ via iTEBD for the $\Delta$ chain for different $J'/J$ at $T = 0$. Note that, for $J \sim 336$ K, a unit of $h$ corresponds to $\sim$250 T. Inset: magnetization at $J'/J = 0.3$ for maximal Schmidt rank $\chi_m = 80(100)$ lines (crosses) and imaginary time $\tau = n_\tau d\tau$, $d\tau = 0.01/J$. (d) MFA for 3D coupled $\Delta$ chains.

reaches up to highest measured fields and is not perfectly flat, but rising at a rate of 0.001 $\mu_B$/T.

From our data, we construct the magnetic phase diagram of atacamite for $\mathbf{H} \| b$ (Fig. 4). The AFM phase exists below $T_N$ and up to $\sim$30 T. It is separated into a low-field regime with the magnetic structure described before and a high-field regime for fields above the spin-flop transition. In the limit $T \to 0$ K, the suppression of AFM order possibly coincides with the appearance of a magnetization plateau-like behavior. To fully establish the magnetic phase diagram in this field region, it requires a determination of the magnetocaloric effect in pulsed magnetic fields [59,60]. At highest fields of 65 T the system is still far from saturation.
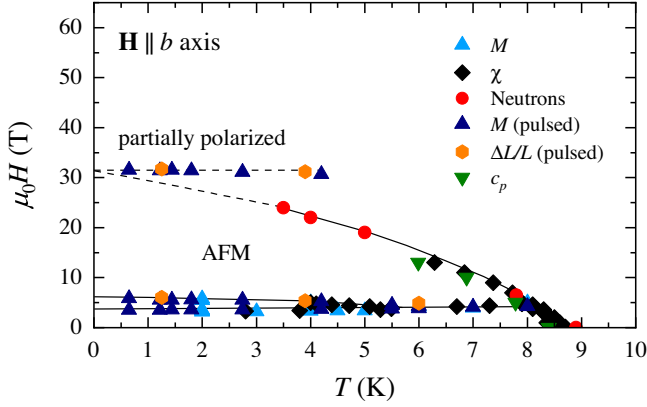
FIG. 4. Magnetic phase diagram of atacamite for $\mathbf{H}\|b$; for details, see text. Data points at 31.5 T from pulsed-field experiments as measured, not corrected for magnetocaloric effect [60].

It is now instructive to establish the Hamiltonian of atacamite and connect it to the observations. To this end, we used an energy mapping technique [61–63] to calculate 17 exchange interactions, derived from the first three coordination shells of the parent pyrochlore structure [42]. Only six of them exceed 1 K, or 0.3% of the dominant coupling $J_4$ [Fig. 1(c)]. A Curie-Weiss temperature $\Theta_{CW}$ calculated from our $J$'s for $U = 8.24$ eV, typical for Cu$^{2+}$, matches the experiment [40,52]. Two antiferromagnetic interactions stand out: $J_4 = 336$ and $J_3 = 102$ K, which bind Cu(1) and Cu(2) atoms into anisotropic $\Delta$ chains [compare Eq. (1) with $J \equiv J_4$ and $J' \equiv J_3$].

Based on these findings, we consider a single $\Delta$ chain [Eq. (1)]. Figure 3(c) shows iTEBD results; complementary ED results are described in the Supplemental Material [42]. For $0.5 \leq J'/J \leq 2$, we observe the famous quantum half-magnetization plateau [26,28,64]. However, it is practically invisible for $J'/J \lesssim 0.5$, relevant for atacamite. Moreover, its field scale is of $O(J) \sim O(250$ T$)$. Therefore, while tempting, the observed flattening of $M(H)$ around 31.5 T in atacamite is *not* related to the half-magnetization plateau physics. On the other hand, the 3D exchange among the chains proves to be relevant. The second finding in Fig. 3(c) is far more striking and has not been appreciated before: in the small-$J'$ gapless phase, e.g., at $J'/J = 0.5$, the low-$h$ susceptibility appears singular and the magnetization approaches a *nonquantized finite* value as $h \to 0$. For the relevant $J'/J \sim 0.3$, the inset of Fig. 3(c) shows iTEBD versus increasing imaginary simulation times $\tau = n_\tau d\tau$ in terms of $d\tau = 0.01/J$. Since iTEBD inherits the limit of system size $N \to \infty$ by construction, and by identifying $\tau^{-1} \sim T$ with a quasitemperature, we extract the following order of limits $\lim_{h\to 0} \lim_{N\to\infty} \langle S^z \rangle_T := M_0(T)$ from the inset. For $T \neq 0$, we find $M_0(T) = 0$, however, as $T \to 0$, very likely, $M_0(T = 0)/\text{cell} \approx 0.435 \neq 0$, all of which is consistent with Mermin-Wagner's theorem. Rephrasing, we seem to observe ferromagnetic order at $T = 0$ for the $\Delta$ chain at $J'/J \sim 0.3$. This likely holds for

the entire small-$J'$ gapless phase. This is consistent with ED [42] and with a classical treatment of the $\Delta$ chain.

In the MFA, the ground state of a single $\Delta$ chain has the same pattern as observed experimentally, with $\theta = 360° - 2 \arccos(-(J'/2J)) = 162.5°$, in excellent agreement with our neutron data, with the Cu$^{2+}$ net moment, $M_{\text{eff}} = (M_2 - M_1 J'/2J)/2$ [42]. If the moment of each copper is taken to be $M_2 = M_1 = 1$ $\mu_B$, then $M_{\text{eff}}^{\text{MFA}} = 0.42$ $\mu_B$. We know from experiment though that these moments are suppressed by fluctuations to $M_1 = 0.34$ $\mu_B$, $M_2 = 0.59$ $\mu_B$. This reduces the net moment to $M_{\text{eff}}(H = 0) = 0.27$ $\mu_B$/Cu [42]. On the other hand, $M_{\text{eff}}^{\text{MFA}} = 0.42$ $\mu_B$ agrees very well with the magnetization at $\sim 30$ T, indicating that in such fields the fluctuations are mostly quenched. In the following, we used $M_{\text{eff}}(H)$ and $M_{1,2}(H)$ linearly interpolating between the two limits.

We are now in a position to describe an effective 3D magnetic model that can be addressed by classical mean-field calculations. These treat the $\Delta$ chains as emergent, rigid macroscopic objects, carrying a large magnetic moment. Classically, the latter arises primarily from Cu(2) moments being aligned ferromagnetically along $b$ [Fig. 1(b)]. These large moments are AFM stacked into a 2D crystal and coupled via the small subleading exchange interactions. Their projection onto the $ac$ plane forms an anisotropic triangular lattice with three effective AFM couplings, $J_B \lesssim J_A \ll J_C$ [42]. For our selected value of $U = 8.24$ eV, $J_C \approx 8$, $J_A \approx 0.5$, and $J_B \approx 0$ K. The classical ground state of this model is collinear with Néel order along $C$ and $B$, and ferromagnetic order along $A$, as observed experimentally [Fig. 1(b)]. We note, however, that $J_{A,B}$ rapidly rise with decreasing $U$, and at $U = 7$ eV (still an admissible value for Cu$^{2+}$) $J_A \approx J_B \approx J_C \approx 10$ K. In that case, the MFA ground state would have been the 120° order.

We focus on the 2D collinear Néel order along the $C$ direction. Since $b$ is the easy axis, the MFA predicts a spin flop at low fields $\mathbf{H}\|b$, whereupon all magnetic moments rigidly rotate so that the Cu(2) moments are $\perp \mathbf{H}$. The classical spin-flop field is $\mu_0 H_1 = M_2(0)/M_{\text{eff}}(0)\sqrt{2KJ_{\Delta-\Delta}}$, where $K$ measures the uniaxial anisotropy (given here for simplicity as an effective single-site term), and the effective coupling $J_{\Delta-\Delta} \approx J_C + J_B \approx 8.5$ K for $U = 8.24$ eV. To reproduce the experimentally observed $\mu_0 H_1 \sim 3.5$ T, one needs $K \sim 0.04$ K (a typical energy scale for Cu$^{2+}$ [65]). The low symmetry of atacamite allows also for some in-plane magnetic anisotropy. A possible splitting of $H_1$ into two close transitions likely reflects such anisotropies.

As the field increases, the spin-flopped state gradually cants, generating a net magnetic moment of $HM_{\text{eff}}^2(H)/M_2^2(H)J_{\Delta-\Delta}$. In an uncorrected MFA, $M(H)$ is linear. However, accounting for quantum fluctuations and their gradual quenching with field leads to deviation from linearity. These deviations are visible in experiment (see

Supplemental Material [42]). At a field $H_2$ the moments cant into the "plateau" configuration, where all $\Delta$ chains are ordered ferromagnetically, and the total moment is $M = M_{\text{eff}}^{\text{MFA}}$. For our calculated parameters, $\mu_0 H_2 = 30.1$ T, to be compared to the experimental value of 31.5 T. In this state, the total moment does not remain constant but keeps rising as $M_{\text{eff}}(H) = (1/2 - J'/4J + H/4J) \, \mu_B$. The differential susceptibility $dM/dH$, calculated this way, is much smaller than in the experiment, yet is qualitatively consistent with the latter [42].

The overall dependence of $M(H)$ as calculated in MFA, adjusted for the quenching of the fluctuations, and using the DFT exchange couplings, exhibits an excellent agreement with the experiment [Fig. 3(d)], giving credence to the calculation and to the described scenario.

Finally, let us discuss the finite-$T$ phase diagram. Since temperature effects might slightly change the ratios between $J_A, J_B$, and $J_C$, we note that a tuning toward the region $J_A \approx J_B \approx J_C$ opens the possibility of multiple phases with various degrees of noncollinearity, some of them only emerging at finite temperatures [2]. While our current observations do not yield hints as to the specific nature of this phase, we note that the phase diagram for the simple isotropic triangular lattice is similar to our Fig. 4 (see Fig. 3 in Ref. [2]). This is a subject for future investigations.

We have studied the natural mineral $Cu_2Cl(OH)_3$ and found that it is well described as a weakly coupled asymmetric triangular lattice of $S = 1/2$ $\Delta$ chains. We find an unusual magnetic behavior, with a magnetization deceivingly reminiscent of the quantum half-magnetization plateau, which, however, turns out to be a classical effect, well described by MFA. A magnetic Hamiltonian derived from first-principles calculations predicts a spin flop, a magnetization plateau, and weak deviation from the plateau behavior in high fields. This compound therefore represents a unique example of strongly coupled 1D ferromagnetic objects coordinated by weak and anisotropic 2D interactions. We hope that this discovery will encourage more studies of this class of magnetic models.

*Corresponding author.
l.heinze@tu-braunschweig.de
†Present address: Physikalisch-Technische Bundesanstalt, 38116 Braunschweig, Germany.

[1] C. Lacroix, P. Mendels, and F. Mila, *Introduction to Frustrated Magnetism*, Springer Series in Solid-State Sciences (Springer-Verlag, Berlin, 2011).

[2] O. A. Starykh, Unusual ordered phases of highly frustrated magnets: A review, Rep. Prog. Phys. **78**, 052502 (2015).

[3] J. Wosnitza, S. A. Zvyagin, and S. Zherlitsyn, Frustrated magnets in high magnetic fields—selected examples, Rep. Prog. Phys. **79**, 074504 (2016).

[4] L. Savary and L. Balents, Quantum spin liquids: A review, Rep. Prog. Phys. **80**, 016502 (2017).

[5] A. B. Harris, C. Kallin, and A. J. Berlinsky, Possible Néel orderings of the kagomé antiferromagnet, Phys. Rev. B **45**, 2899 (1992).

[6] K. Takano, K. Kubo, and H. Sakamoto, Ground states with cluster structures in a frustrated Heisenberg chain, J. Phys. Condens. Matter **8**, 6405 (1996).

[7] T. Tonegawa and I. Harada, Ground-state properties of the one-dimensional isotropic spin-1/2 Heisenberg antiferromagnet with competing interactions, J. Phys. Soc. Jpn. **56**, 2153 (1987).

[8] A. Olariu, P. Mendels, F. Bert, F. Duc, J. C. Trombe, M. A. de Vries, and A. Harrison, $^{17}O$ NMR Study of the Intrinsic Magnetic Susceptibility and Spin Dynamics of the Quantum Kagome Antiferromagnet $ZnCu_3(OH)_6Cl_2$, Phys. Rev. Lett. **100**, 087202 (2008).

[9] H. Kikuchi, Y. Fujii, M. Chiba, S. Mitsudo, T. Idehara, T. Tonegawa, K. Okamoto, T. Sakai, T. Kuwai, and H. Ohta, Experimental Observation of the 1/3 Magnetization Plateau in the Diamond-Chain Compound $Cu_3(CO_3)_2(OH)_2$, Phys. Rev. Lett. **94**, 227201 (2005).

[10] K. C. Rule, D. A. Tennant, J.-S. Caux, M. C. R. Gibson, M. T. F. Telling, S. Gerischer, S. Süllow, and M. Lang, Dynamics of azurite $Cu_3(CO_3)_2(OH)_2$ in a magnetic field as determined by neutron scattering, Phys. Rev. B **84**, 184419 (2011).

[11] H. O. Jeschke, I. Opahle, H. Kandpal, R. Valentí, H. Das, T. Saha-Dasgupta, O. Janson, H. Rosner, A. Brühl, B. Wolf, M. Lang, J. Richter, S. Hu, X. Wang, R. Peters, Th. Pruschke, and A. Honecker, Multistep Approach to Microscopic Models for Frustrated Quantum Magnets: The Case

of the Natural Mineral Azurite, Phys. Rev. Lett. **106,** 217201 (2011).

[12] B. Willenberg, M. Schäpers, A. U. B. Wolter, S.-L. Drechsler, M. Reehuis, J.-U. Hoffmann, B. Büchner, A. J. Studer, K. C. Rule, B. Ouladdiaf, S. Süllow, and S. Nishimoto, Complex Field-Induced States in Linarite $PbCuSO_4(OH)_2$ with a Variety of High-Order Exotic Spin-Density Wave States, Phys. Rev. Lett. **116,** 047202 (2016).

[13] D. Inosov, Quantum magnetism in minerals, Adv. Phys. **67,** 149 (2018).

[14] T. Hamada, J. Kane, S. Nakagawa, and Y. Natsume, Exact solution of ground state for uniformly distributed RVB in one-dimensional spin-1/2 Heisenberg systems with frustration, J. Phys. Soc. Jpn. **57,** 1891 (1988).

[15] K. Kubo, Excited states and the thermodynamics of a fully frustrated quantum spin chain, Phys. Rev. B **48,** 10552 (1993).

[16] H. Otsuka, Thermodynamic properties of the $\Delta$-chain model in a uniform magnetic field, Phys. Rev. B **51,** 305 (1995).

[17] T. Nakamura and Y. Saika, Thermodynamic property of the $\Delta$-chain, J. Phys. Soc. Jpn. **64,** 695 (1995).

[18] T. Nakamura and K. Kubo, Elementary excitations in the $\Delta$ chain, Phys. Rev. B **53,** 6393 (1996).

[19] D. Sen, B. S. Shastry, R. E. Walstedt, and R. Cava, Quantum solitons in the sawtooth lattice, Phys. Rev. B **53,** 6401 (1996).

[20] K. Maisinger and U. Schollwöck, Thermodynamics of Frustrated Quantum Spin Chains, Phys. Rev. Lett. **81,** 445 (1998).

[21] S. A. Blundell and M. D. Nùñez-Regueiro, Quantum topological excitations: From the sawtooth lattice to the Heisenberg chain, Eur. Phys. J. B **31,** 453 (2003).

[22] M. E. Zhitomirsky and H. Tsunetsugu, Exact low-temperature behavior of a kagomé antiferromagnet at high fields, Phys. Rev. B **70,** 100403(R) (2004).

[23] T. Tonegawa and M. Kaburagi, Ground-state properties of an $S = \frac{1}{2}$ $\Delta$-chain with ferro- and antiferromagnetic interactions, J. Magn. Magn. Mater. **272–276,** 898 (2004).

[24] O. Derzhko and J. Richter, Finite low-temperature entropy of some strongly frustrated quantum spin lattices in the vicinity of the saturation field, Phys. Rev. B **70,** 104415 (2004).

[25] V. R. Chandra, D. Sen, N. B. Ivanov, and J. Richter, Antiferromagnetic sawtooth chain with spin-$\frac{1}{2}$ and spin-1 sites, Phys. Rev. B **69,** 214406 (2004).

[26] J. Richter, J. Schulenburg, A. Honecker, J. Schnack, and H.-J. Schmidt, Exact eigenstates and macroscopic magnetization jumps in strongly frustrated spin lattices, J. Phys. Condens. Matter **16,** S779 (2004).

[27] Y. Inagaki, Y. Narumi, K. Kindo, H. Kikuchi, T. Kamikawa, T. Kunimoto, S. Okubo, H. Ohta, T. Saito, M. Azuma, M. Takano, H. Nojiri, M. Kaburagi, and T. Tonegawa, Ferro-antiferromagnetic delta-chain system studied by high field magnetization measurements, J. Phys. Soc. Jpn. **74,** 2831 (2005).

[28] J. Richter, O. Derzhko, and A. Honecker, The sawtooth chain: From Heisenberg spins to Hubbard electrons, Int. J. Mod. Phys. B **22,** 4418 (2008).

[29] K. Hida, Exotic ground state phases of $S = \frac{1}{2}$ Heisenberg $\Delta$-chain with ferromagnetic main chain, J. Phys. Soc. Jpn. **77,** 044707 (2008).

[30] Z. Hao, Y. Wan, I. Rousochatzakis, J. Wildeboer, A. Seidel, F. Mila, and O. Tchernyshyov, Destruction of valence-bond order in a $S = \frac{1}{2}$ sawtooth chain with a Dzyaloshinskii-Moriya term, Phys. Rev. B **84,** 094452 (2011).

[31] V. Ya. Krivnov, D. V. Dmitriev, S. Nishimoto, S.-L. Drechsler, and J. Richter, Delta chain with ferromagnetic and antiferromagnetic interactions at the critical point, Phys. Rev. B **90,** 014441 (2014).

[32] D. V. Dmitriev and V. Ya. Krivnov, Delta chain with anisotropic ferromagnetic and antiferromagnetic interactions, Phys. Rev. B **92,** 184422 (2015).

[33] D. V. Dmitriev and V. Ya. Krivnov, Ferrimagnetism in delta chain with anisotropic ferromagnetic and antiferromagnetic interactions, J. Phys. Condens. Matter **28,** 506002 (2016).

[34] D. V. Dmitriev and V. Ya. Krivnov, Heisenberg-Ising delta-chain with bond alternation, J. Phys. Condens. Matter **30,** 385803 (2018).

[35] O. Le Bacq, A. Pasturel, C. Lacroix, and M. D. Nùñez-Regueiro, First-principles determination of exchange interactions in delafossite $YCuO_{2.5}$, Phys. Rev. B **71,** 014432 (2005).

[36] H. Kikuchi, Y. Fujii, D. Takahashi, M. Azuma, Y. Shimakawa, T. Taniguchi, A. Matsuo, and K. Kindo, Spin gapped behavior of a frustrated delta chain compound euchroite, J. Phys. Conf. Ser. **320,** 012045 (2011).

[37] A. Baniodeh, N. Magnani, Y. Lan, G. Buth, C. Anson, J. Richter, M. Affronte, J. Schnack, and A. K. Powell, High spin cycles: Topping the spin record for a single molecule verging on quantum criticality, npj Quantum Mater. **3,** 10 (2018).

[38] H. O. Jeschke, H. Nakano, and T. Sakai, From kagome strip to kagome lattice: Realizations of frustrated $S = 1/2$ antiferromagnets in Ti(III) fluorides, Phys. Rev. B **99,** 140410 (R) (2019).

[39] Helmholtz-Zentrum Berlin für Materialien und Energie, E2: The flat-cone diffractometer at BER II, J. Large-Scale Res. Facil. **4,** A129 (2018).

[40] L. Heinze, R. Beltran-Rodriguez, G. Bastien, A. U. B. Wolter, M. Reehuis, J.-U. Hoffmann, K. C. Rule, and S. Süllow, The magnetic properties of single-crystalline atacamite, $Cu_2Cl(OH)_3$, Physica (Amsterdam) **536B,** 377 (2018).

[41] Helmholtz-Zentrum Berlin für Materialien und Energie, HFM/EXED: The high magnetic field facility for neutron scattering at BER II, J. Large-Scale Res. Facil. **3,** A115 (2017).

[42] See Supplemental Material at http://link.aps.org/supplemental/10.1103/PhysRevLett.126.207201 for additional information on the characterization of the atacamite single crystals and the neutron diffraction experiments for crystal and magnetic structure determination. Further, we provide additional information on the electronic structure calculations as well as the classical mean-field theory of an individual $\Delta$ chain and a collection of chains. We also present additional experimental data probing the metamagnetic transition and theoretical results for a sawtooth chain with additional in-chain coupling, as well as exact diagonalization results for the $\Delta$ chain. The Supplemental Material includes Ref. [43].

[43] M. E. Zhitomirsky and T. Nikuni, Magnetization curve of a square-lattice Heisenberg antiferromagnet, Phys. Rev. B **57,** 5013 (1998).

[44] *Xtal 3.4 User's Manual*, edited by R. Hall, G. S. D. King, and J. M. Stewart (University of Australia, Lamb, Perth, 1995).

[45] V. F. Sears, in *International Tables for Crystallography*, edited by A. J. C. Wilson (Kluwer Academic Publishers, Dordrecht, 1995), Vol. C, p. 383.

[46] P. J. Brown, in *International Tables for Crystallography*, edited by A. J. C. Wilson (Kluwer Academic Publishers, Dordrecht, 1995), Vol. C, p. 391.

[47] K. Koepernik and H. Eschrig, Full-potential nonorthogonal local-orbital minimum-basis band-structure scheme, Phys. Rev. B **59**, 1743 (1999).

[48] J. P. Perdew, K. Burke, and M. Ernzerhof, Generalized Gradient Approximation Made Simple, Phys. Rev. Lett. **77**, 3865 (1996).

[49] A. I. Liechtenstein, V. I. Anisimov, and J. Zaanen, Density-functional theory and strong interactions: Orbital ordering in Mott-Hubbard insulators, Phys. Rev. B **52**, R5467 (1995).

[50] G. Vidal, Classical Simulation of Infinite-Size Quantum Lattice Systems in One Spatial Dimension, Phys. Rev. Lett. **98**, 070201 (2007).

[51] J. B. Parise and B. G. Hyde, The structure of atacamite and its relationship to spinel, Acta Crystallogr. C **42**, 1277 (1986).

[52] X. G. Zheng, T. Mori, K. Nishiyama, W. Higemoto, H. Yamada, K. Nishikubo, and C. N. Xu, Antiferromagnetic transitions in polymorphous minerals of the natural cuprates atacamite and botallackite $Cu_2Cl(OH)_3$, Phys. Rev. B **71**, 174404 (2005).

[53] X. G. Zheng and E. S. Otabe, Antiferromagnetic transition in atacamite $Cu_2Cl(OH)_3$, Solid State Commun. **130**, 107 (2004).

[54] K. Zenmyo, H. Kubo, M. Tokita, T. Hamasaki, M. Hagihala, X.-G. Zheng, T. Kawae, Y. Takeuchi, and M. Matsumura, Proton NMR study of atacamite $Cu_2Cl(OH)_3$, J. Phys. Soc. Jpn. **82**, 084707 (2013).

[55] From an analysis of the low-temperature magnetic susceptibility of several atacamite samples, we estimate that the amount of $S = 1/2$ impurities is less than 0.5%, as indicated by the absence of a Curie tail down to the lowest experimental temperature of $T = 2$ K [see Fig. 2(b)].

[56] E. F. Bertaut, Representation analysis of magnetic structures, Acta Crystallogr. A **24**, 217 (1968).

[57] M. Jaime, C. C. Moya, F. Weickert, V. Zapf, F. Balakirev, M. Wartenbe, P. Rosa, J. Betts, G. Rodriguez, S. Crooker, and R. Daou, Fiber Bragg grating dilatometry in extreme magnetic field and cryogenic conditions, Sensors **17**, 2572 (2017).

[58] J. A. Detwiler, G. M. Schmiedeshoff, N. Harrison, A. H. Lacerda, J. C. Cooley, and J. L. Smith, Magnetization of $UBe_{13}$ to 60 T, Phys. Rev. B **61**, 402 (2000).

[59] T. Nomura, Y. Skourski, D. L. Quintero-Castro, A. A. Zvyagin, A. V. Suslov, D. Gorbunov, S. Yasin, J. Wosnitza, K. Kindo, A. T. M. N. Islam, B. Lake, Y. Kohama, S. Zherlitsyn, and M. Jaime, Enhanced spin correlations in the Bose-Einstein condensate compound $Sr_3Cr_2O_8$, Phys. Rev. B **102**, 165144 (2020).

[60] Recently, we became aware of the existence of a strong magnetocaloric effect (MCE) in atacamite that might cause the sample to be adiabatically (as opposed to isothermically) magnetized in pulsed magnetic fields, even when immersed in liquid He at cryogenic temperatures. A detailed MCE study, outside of the scope of the present Letter, is currently under way to establish the $(T, \mu_0 H)$ phase diagram of this material beyond ambiguities.

[61] J. K. Glasbrenner, I. I. Mazin, H. O. Jeschke, P. J. Hirschfeld, R. M. Fernandes, and R. Valentí, Effect of magnetic frustration on nematicity and superconductivity in iron chalcogenides, Nat. Phys. **11**, 953 (2015).

[62] Y. Iqbal, T. Müller, H. O. Jeschke, R. Thomale, and J. Reuther, Stability of the spiral spin liquid in $MnSc_2S_4$, Phys. Rev. B **98**, 064427 (2018).

[63] P. Ghosh, Y. Iqbal, T. Müller, R. Thomale, J. Reuther, M. J. P. Gingras, and H. O. Jeschke, Breathing chromium spinels: A showcase for a variety of pyrochlore Heisenberg Hamiltonians, npj Quantum Mater. **4**, 63 (2019).

[64] A. Metavitsiadis, C. Psaroudaki, and W. Brenig, Enhancement of magnetization plateaus in low-dimensional spin systems, Phys. Rev. B **101**, 235143 (2020).

[65] J. M. Tranquada, G. Shirane, B. Keimer, S. Shamoto, and M. Sato, Neutron scattering study of magnetic excitations in $YBa_2Cu_3O_{6+x}$, Phys. Rev. B **40**, 4503 (1989).